



Development of a GPS deterministic multipath simulator for an efficient computation of the positioning errors

Adrien Chen, Alexandre Chabory, Anne-Christine Escher, Christophe Macabiau

► To cite this version:

Adrien Chen, Alexandre Chabory, Anne-Christine Escher, Christophe Macabiau. Development of a GPS deterministic multipath simulator for an efficient computation of the positioning errors. ION GNSS 2009, 22nd International Technical Meeting of The Satellite Division of the Institute of Navigation, Sep 2009, Savannah, United States. pp 2378-2390. hal-01022159

HAL Id: hal-01022159

<https://enac.hal.science/hal-01022159>

Submitted on 23 Sep 2014

HAL is a multi-disciplinary open access archive for the deposit and dissemination of scientific research documents, whether they are published or not. The documents may come from teaching and research institutions in France or abroad, or from public or private research centers.

L'archive ouverte pluridisciplinaire **HAL**, est destinée au dépôt et à la diffusion de documents scientifiques de niveau recherche, publiés ou non, émanant des établissements d'enseignement et de recherche français ou étrangers, des laboratoires publics ou privés.

Development of a GPS Deterministic Multipath Simulator for an Efficient Computation of the Positioning Errors

Adrien CHEN, Alexandre CHABORY, Anne-Christine ESCHER, Christophe MACABIAU, ENAC, Toulouse, France

BIOGRAPHY

Adrien CHEN graduated as an electronics engineer in 2007 from the ENAC (Ecole Nationale de l'Aviation Civile) in Toulouse, France. Since 2007, he is a PhD student at the signal processing lab of ENAC working on multipath modeling for civil aviation.

Dr. Alexandre CHABORY graduated in 2001 as an electronics engineer from the ENAC. From 2001 to 2004, he was a PhD student at ONERA. From 2004 to 2007, he was a postdoctoral scientist with the Eindhoven University of Technology (TU/e). Since 2007, he is an assistant professor with the ENAC electromagnetics lab. His research interests mainly deal with electromagnetic theory, modeling and applications.

Dr. Anne-Christine ESCHER graduated as an electronics engineer in 1999 from the ENAC in Toulouse, France. Since 2002, she has been working as an associate researcher in the signal processing lab of the ENAC. She received her Ph.D. in 2003.

Dr. Christophe MACABIAU graduated as an electronics engineer in 1992 from the ENAC in Toulouse, France. Since 1994, he has been working on the application of satellite navigation techniques to civil aviation. He received his PhD in 1997 and has been in charge of the signal processing lab of ENAC since 2000.

ABSTRACT

Multipath is defined by echoes associated with the fields reflected by the surrounding environment. In multipath situations, the received signal is not only the direct one but also a sum of attenuated and delayed versions of the direct signal. For this reason, a multipath channel is usually characterized by a set of four parameters: the amplitude, the delay, the phase shift and the Doppler shift of each multipath. When characterizing a multipath channel, the main issue is the prediction of these parameters.

In this paper, we propose a GPS multipath prediction simulator adapted to airport navigation which can predict the GPS multipath error in static and dynamic configurations. This simulator consists in a multipath generator and a GPS receiver simulator. It takes into account the 3D environment, the satellite and receiver positions. Concerning the electromagnetic modeling we show that ray methods should not be used for GPS multipath prediction if few-meters objects are present in the environment. Next, the choice of physical optics (PO) is numerically validated via comparisons with the method of moments (MoM). We also show that the computation of multiple reflections up to order 2 is sufficient. We present techniques that improve the computation efficiency of the simulator. Finally a test case is exposed.

I.INTRODUCTION

From the satellite to the receiver antenna, the GPS signal is confronted to a number of propagation effects which may constitute sources of positioning error. For instance, when passing through the atmosphere, the signal undergoes ionospheric and tropospheric effects which affect its magnitude and delay. Among the different propagation phenomena, multipath has been identified in the literature as the most challenging source of positioning error in man-made environments. Therefore, it is important to get information about the potential multipath affecting the signal reception. This is particularly the case when precise positioning is required.

Numbers of multipath prediction tools already exist. We can distinguish three kinds of models: deterministic models [1]-[2], statistic models [3]-[4] and finally hybrid models which mix both deterministic and statistic prediction [5]-[7]. Here we focus on deterministic models. When defining a multipath prediction simulator, many possibilities are available at each stage of the conception [8], and it appears that the best solutions may not be obvious. For instance, the choice of an electromagnetic prediction method, the number of interactions to consider

or suitable criteria for the 3D environment description are of major concerns.

In this paper, we propose a GPS multipath prediction simulator based on PO adapted to airport navigation for which we aim at justifying each design choice carefully.

In the second section we expose the simulator principle. In the third section we justify the prediction method employed in the multipath generator by means of comparisons with other approaches: geometrical optics (GO), the uniform theory of diffraction (UTD) and the method of moments (MoM). In the fourth section we present the choices and techniques used in the simulator in order to improve its computation efficiency. Finally, in the fifth section we present a test-case simulation.

II.FEATURES OVERVIEW

Global structure

The simulator is composed of two blocks, the multipath generator which predicts the channel parameters and the GPS receiver simulator which returns the position error. Its principle is illustrated in Figure 1.

The input parameters of the multipath generator are the satellite position, the receiver position, and the 3D modeling of the environment composed of planar dielectric and metallic facets. The role of the multipath generator is to predict the channel parameters. These parameters become the input of the GPS receiver simulator which returns the range estimation error between the satellite and the receiver due to multipath.

The multipath generator contains two main parts. The first one predicts the list of the electromagnetic fields associated with each multipath. These fields are computed by PO. The second one simulates the GPS receiver antenna. It allows the computation of the multipath parameters from the electromagnetic fields via the use of the effective vectorial height of the antenna.

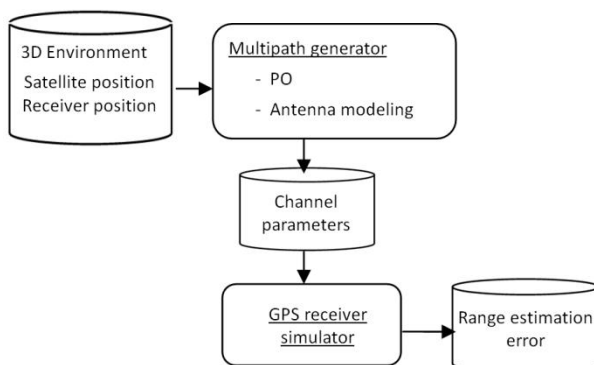


Figure 1 Principle of the coupling between the multipath generator and the GPS receiver simulator

Static and dynamic simulations

Simulations can be performed either in static or in dynamic configurations.

In static configurations, the receiver and satellite are static. Hence, the inputs of the simulator are assumed time-invariant. The prediction results can be displayed in two different ways. The first possibility is to display results at points sampled on a segment as illustrated in Figure 2.

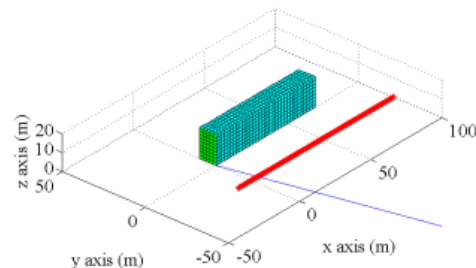


Figure 2 Computation at points along a segment

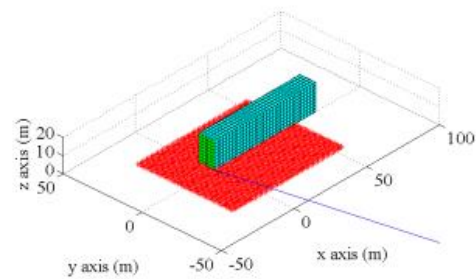


Figure 3 Computation in a plane

The second possibility is to display the results at points sampled in a plane as illustrated in Figure 3.

A simulation is dynamic when either the receiver or the satellite are moving. The input parameters become time-variant. The predictions are displayed along a trajectory of the receiver.

Satellite Constellation

The simulation is mono-channel which means that the prediction is done for one satellite. The position of the satellite can be determined in two ways. It can either be a position defined by its elevation, azimuth and range. Alternatively, the satellite can be chosen among the GPS constellation. In this case, the GPS time of simulation has to be known, and the satellite position is computed from the almanacs.

Scene Modeling

The environment has to be modeled in 3 dimensions. The 3D modeling has to be composed of rectangular or triangular facets.

Multipath computation

The aim of this section is to present the computation of the multipath parameters. These parameters are (a_k, τ_k, ϕ_k) , the amplitude (or gain), arrival time and phase of the k -th path, respectively. In dynamic simulations, there is an additional parameter, the Doppler shift f_k^D of each multipath which also has to be computed. In such simulations the multipath parameters become $(a_k, \tau_k, \phi_k, f_k^D)$. These parameters describe entirely the multipath channel.

The fields scattered by the facets are computed via an approach based on PO up to second order reflections. This approach is detailed and justified in Section III of this paper. Once the scattered fields have been predicted in one point, the multipath parameters remain to be computed.

The multipath parameters (a_k, ϕ_k) are computed for each illuminated facet from the electromagnetic fields via the use of the effective vectorial height of the antenna. An omnidirectional antenna or a realistic antenna can be chosen.

In the electromagnetic computation, everything is done as if the GPS signal were monofrequential of frequency $f = f_{L1}$, i.e. a pure sinusoidal signal. This is the harmonic hypothesis. Hence, for each illuminated facet, the multipath parameters (a_k, ϕ_k) are computed at f_{L1} . Besides, τ_k are the geometric delays. For the direct signal, τ_1 is the geometrical delay between the satellite and the receiver. For the multipath, τ_k are also the geometrical delays of each multipath. These delays are related to the distances between the satellite, the center of the illuminated facets and the receiver.

If $x(t)$ represents the waveform emitted by a satellite, the received signal $y(t)$ is a sum of attenuated, time-delayed versions of $x(t)$. Here we use the classical impulse response function $h(t)$ for multipath channels given by:

$$h(t) = \sum_{k=1}^K a_k \delta(t - \tau_k) e^{j\phi_k}. \quad \text{Eq. 1}$$

This gives in the frequency domain

$$H(f) = \sum_{k=1}^K a_k e^{-j2\pi f \tau_k} e^{j\phi_k}. \quad \text{Eq. 2}$$

Hence, the electromagnetic computation has been done at f_{L1} , but the delays τ_k actually induce a frequency dependence of the channel. Note that for GPS applications, the frequency band of interest is $B = 24\text{MHz}$. Note also that Eq. 1 and Eq. 2 are only valid in static configurations. The Doppler shifts must be taken into account in dynamic cases.

GPS Receiver simulator

The GPS receiver simulator has been developed by the ENAC. It simulates the correlators outputs which expressions can be found in [9].

Once the multipath parameters are computed, the GPS range error prediction can start. The receiver simulator computes the estimated range between the receiver and the satellite. Hence, by knowing the real range, we deduce the multipath error.

III. PRESENTATION OF THE PO PREDICTION AND CONFRONTATION WITH GO, UTD AND MOM

Most of prediction models ([1]-[2]) predict multipath by combining ray tracing techniques with GO or with UTD. One of the main issues of the development of this simulator was the choice of an electromagnetic theory. The aim of this section is to detail the choice of PO, justifying carefully each step.

First of all we present PO and how it is implanted in the simulator. Then we present the three other prediction methods. Secondly we compare the ability of GO, UTD and PO to produce accurate channel parameters in canonical configurations. Finally we expose the validation of PO. For this purpose we compare the EM prediction of the simulator with predictions computed via FEKO, a commercial electromagnetic software based on the MoM [10].

Prediction based on physical optics

PO is a current asymptotic method valid at high frequencies (the signal wavelength is small in comparison to the size of the reflectors). Within this approach, each illuminated surface generates reflected field. Since the environment is described by a set of facets, each illuminated facet is at the origin of one multipath. In order to reduce the computation time of the surface integral that appears for each facet with PO, we use the Mittra and Lee method [11].

The simulator can compute the reflected field for metallic and dielectric multilayer facets and multiple reflections up to order 2. The following explains and illustrates the different reflection orders. For the sake of clarity, the reflection from only one facet is represented in the next figures. The facets of the scene illuminated by the satellite are detected and the reflected fields / multipath are computed at the point(s) of interest with PO. Figure 4 illustrates the first-order reflection computation.

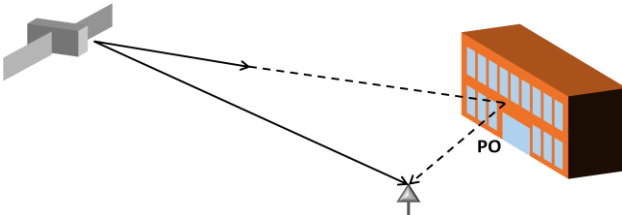


Figure 4 Illustration of first order reflection

Facets illuminated at the first order may illuminate facets at the second order. These facets illuminated at the second order are detected via a ray-tube algorithm. For each facet illuminated at the first order, we define a reflected ray-tube by means of Snell-Descartes laws. The second order illuminated facets are the ones which center is inside this ray-tube as illustrated in Figure 5.

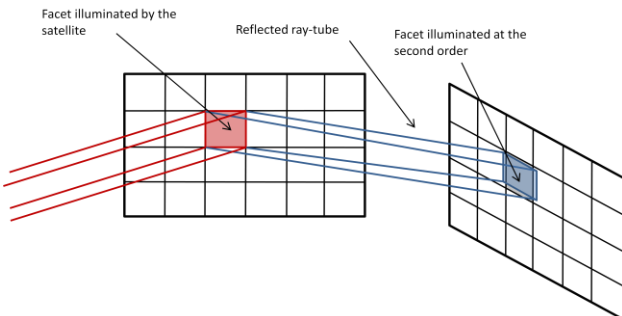


Figure 5 Illustration of the second-order illumination detection

For these facets, the incident field is computed with GO and the reflected field is computed with PO as illustrated in Figure 6.

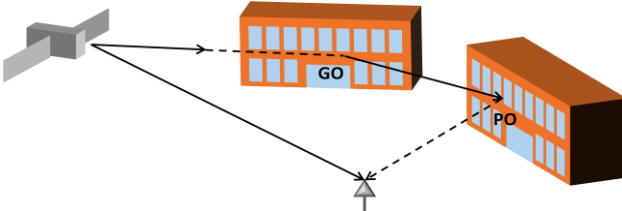


Figure 6 Illustration of second-order reflection

Concerning the ground modeling, there are two ways to compute the ground reflection depending on the type of ground.

When the ground is planar and infinite, the ground reflections up to order 2 are computed by means of the image theorem as illustrated in Figure 7.

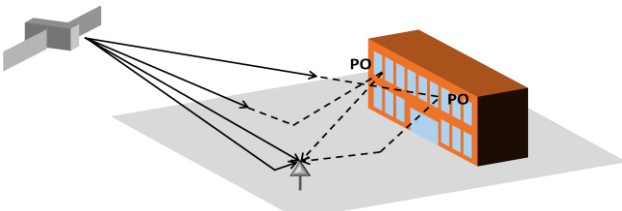


Figure 7 Illustration of planar and infinite ground modeling

When the ground is not flat, it can be modeled with facets. However, the computation time becomes more costly.

To use the technique of [11] within PO, the prediction point has to be in the far field of the facet. Therefore, the facet size D must be chosen small enough so that the distance d between the receiver and a facet respects the condition

$$d > 2D^2/\lambda. \quad \text{Eq. 3}$$

According to Eq. 3, for a chosen size of facets it exists a minimum observation distance, and for a chosen observation distance, it exists a maximum size of facets. Figure 8 illustrates the maximum size of the facets in function of the observation distance.

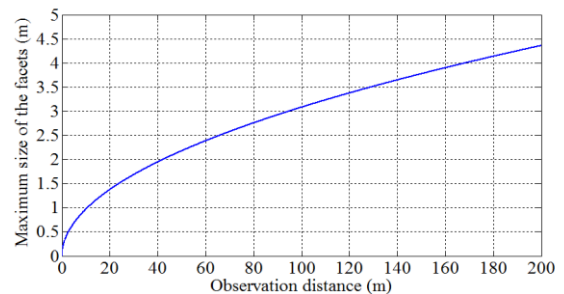


Figure 8 Maximum size of the facets with respect to the observation distance

In the simulator, the mesh can be refined so as to respect this condition. For instance we observe that a facet size of 0.5m insures the validity of the far-field hypothesis for observation distances greater than 3m and a facet size of 1m insures the validity of the far-field hypothesis for observation distances greater than 10m. Hence, according to this criterion, for airport navigation a facet size of 1m is sufficient since the GPS antenna of an airplane is never closer than 10m from the airport environment.

Presentation of the other methods

Ray optics are also based on an asymptotic development of the Maxwell equations valid at high frequencies. These methods rely on ray approximations to compute the propagation and interactions of fields. They are often used for propagation and multipath prediction. In this study we have used two ray methods, GO which only considers reflections on surfaces and UTD which also considers edge diffraction. The simulator allows the computation of the reflected fields with GO and UTD via MUSICA. MUSICA is a GO/UTD prediction software developed by the ENAC [12].

On the other hand, MoM is a current exact method. It is considered as a reference method. However, it cannot be systematically used for our application since it would require too much computational efforts. In this paper we use FEKO in order to validate the predictions of our

simulator. FEKO is a commercial electromagnetic analysis software based on the MoM [10]. Besides, it proposes different solution techniques: GO, UTD and PO.

Comparison of PO/UTD/GO

For all the next simulations we consider two canonical scenes. The first one is a large rectangular metallic reflector of size (69.6m x 16.2m), which size corresponds to an ENAC campus building as illustrated by Figure 9. The second scene is a smaller metallic rectangular reflector of size (3.3m x 1.6m), which size may correspond to a window of the preceding building. Reflectors are meshed with rectangular facets of size 0.5m. The antenna is modeled as isotropic, right-hand circularly polarized (RHCP) and with a polarization mismatch factor of -5dB. The incident field coming from the satellite is a RHCP plane wave, with an incidence of azimuth $\phi = 45^\circ$ and elevation $\theta = 0^\circ$.

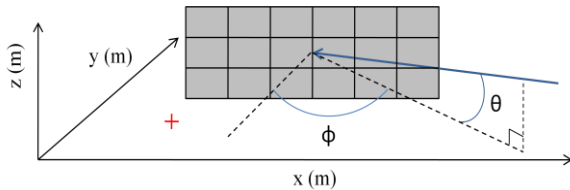


Figure 9 Configuration of the simulations (red dot: receiver position, blue line: direction of incidence)

In Figure 10, we expose the Power Delay Profiles (PDP) $|h(t)|$ (Eq. 1) obtained with the different methods for a receiver located in front of the large metallic reflector.

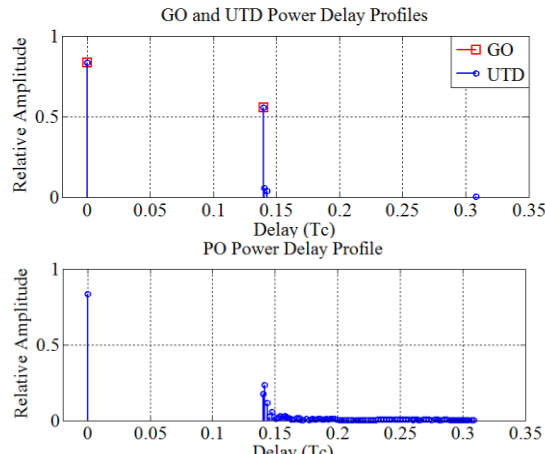


Figure 10 Comparison of the GO, UTD and PO Power Delay Profiles

The UTD PDP highlights the presence of one direct path, followed by one reflected and 4 diffracted multipath. On the other hand, the PO PDP shows one direct path followed by an important number of multipath. Hence, it appears difficult to compare the PDPs of the different channel models. To establish a comparison criterion, a

more suitable way consists in looking at the results in the frequency domain. In Figure 11, we observe the transfer functions obtained with PO, GO and UTD in the GPS frequency band. We denote that the differences between PO and UTD are smaller than with GO.

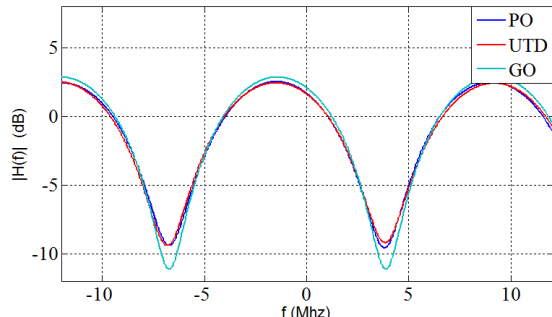


Figure 11 Transfer functions of the GPS multipath channel using the different modeling approaches

In order to have a complete comparison of the channel transfer functions computed with GO, UTD and PO we compute the differences on a plane around the building. For this purpose we define the root mean square difference between two results $h_1(t)$ and $h_2(t)$ as

$$\epsilon_{mq}^2 = \frac{\int_{-B/2}^{B/2} |S_{GPSL1} \cdot (H_1(f) - H_2(f))|^2 df}{\int_{-B}^B |S_{GPSL1}|^2 df}, \quad \text{Eq. 4}$$

with S_{GPSL1} the spectrum envelop of the GPS L1 signal. From the receiver point of view, two models predicting the same transfer functions in the GPS band are strictly equivalent. Notice that we consider that two predictions fit correctly if

$$\epsilon_{mq} \leq -20 \text{dB} \quad \text{Eq. 5}$$

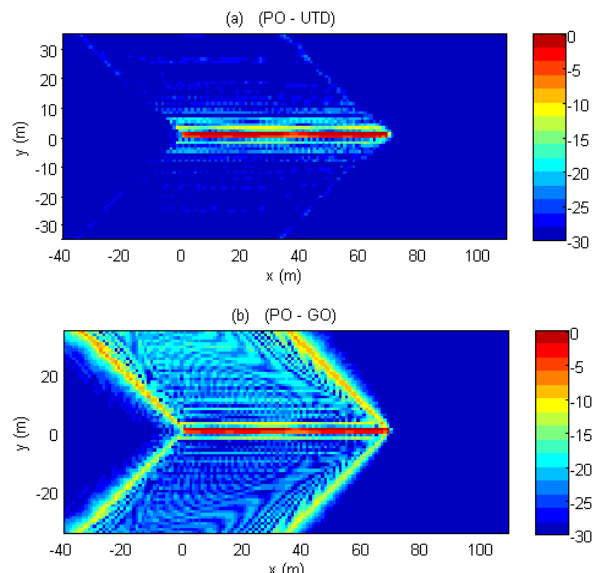


Figure 12 Root mean square difference in dB between: (a) PO and UTD, (b) PO and GO

In Figure 12 (a) we depict ϵ_{mq} in the vicinity of the reflector at a height of 8.1m. We notice that PO and UTD match except at distances below one meter from the reflector where ϵ_{mq} is about 0dB. These significant differences are due to the fact that at this distance, we are not in the far field of the facets as imposed by Eq. 3, thus PO is not valid. To reduce this error in PO, smaller facets can be employed, which will however yield longer computation times. Moreover, for airport navigation, this prediction error is not significant since the GPS antenna of an aircraft will never be as close as one meter from a building. Figure 12 (b) shows large differences between GO and PO near the reflector, and also near the shadow boundaries where ϵ_{mq} can be of order -5dB. Hence, GO produces significant errors near the shadow boundaries. This is an expected result since GO does not take into account edge diffraction.

We now focus on the case where the reflector is smaller. Figure 13 illustrates the field on the axis of specular reflection.

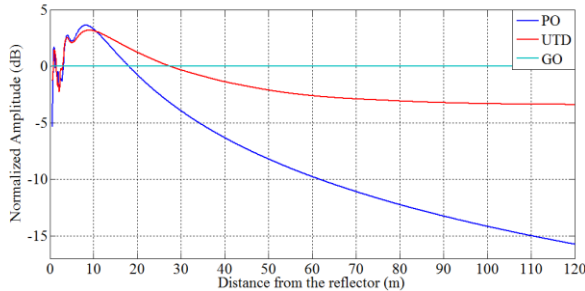


Figure 13 Reflected electric field computed with PO, UTD and GO

In the far-field zone of the reflector, we observe significant differences in the methods. Indeed, only PO gives consistent results, i.e. a field that decreases in $1/r$ with r the distance from the reflector. On the contrary, UTD and GO results are non-physical: we do not observe a $1/r$ decreasing of the reflected field. This phenomenon is explained by the fact that there are caustics in the pencil of reflected and diffracted rays [13]. Indeed, we consider an incident plane wave on a planar object, and we observe in the far-field zone of the reflector.

Hence, the UTD prediction only gives valid results in the near-field zone of the reflector, i.e. approximately for

$$r < \frac{D^2}{2\lambda}. \quad \text{Eq. 6}$$

From the observations made with the precedent simulations, we now discuss the choice of the electromagnetic modeling theory for our simulator.

In the GPS context, for large facades, the multipath area ($r \leq 460$ m) remains in the near-field zone of the object. Notice that the multipath area, which is defined in details in Section V, is the zone inside which the environment

can affect the GPS position because of the presence of multipath. In this configuration we have shown that UTD and PO give similar results while differences exist with GO near the shadow boundaries. For small planar objects, the multipath area may be greater than the near-field zone of the object, inside which we have observed non-physical results with UTD and GO.

Hence, at the maximum observation distance ($r = 460$ m), the minimal acceptable size of objects that GO and UTD can treat may be estimated using Eq. 6 which leads to a limit of about 13m. As explained in [8] objects of size few meters significantly impact the range error. Therefore we cannot employ GO or UTD in the simulator. Finally, we choose to employ PO.

Comparison PO/MoM

In this section we compare PO and MoM in order to validate the PO prediction with a reference method. For the next simulations we use two scenes associated with first and second order reflections. The first scene is a metallic façade of size 3x5m and the second scene is a dihedral composed of two metallic facades of size 3x5m. We compute the scattered field in the specular direction.

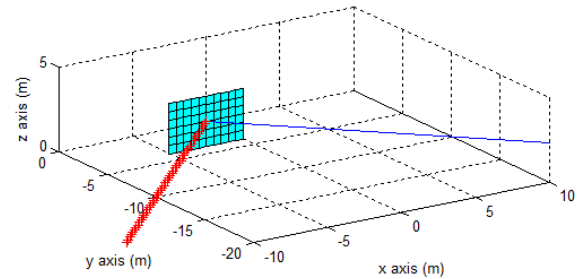


Figure 14 Configuration of scene 1 (red dots: receiver positions, blue line: direction of incidence)

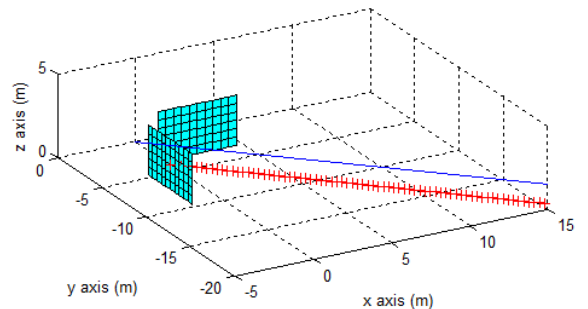


Figure 15 Configuration of scene 2 (red dots: receiver positions, blue line: direction of incidence)

Firstly we present the validation of the first order reflection with FEKO. Figure 16 presents the scattered field computed with the simulator (blue curve), with

FEKO using PO theory (red curve) and with FEKO using MoM theory (black curve).

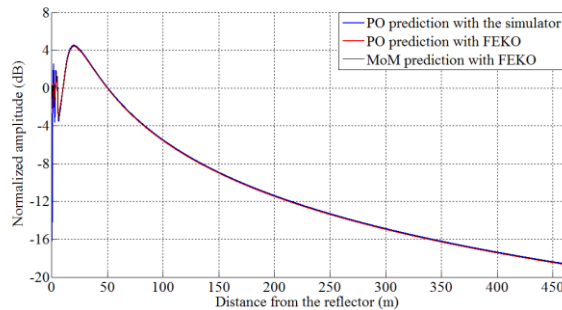


Figure 16 Comparison of the first-order scattered field computed with the simulator (blue), with FEKO using the MoM method (green) and PO method (green) (dB)

We observe that the three curves fit. In order to have a comparison criterion we compute the relative difference between two predicted fields E_1 and E_2 , with reference to the direct field E_0 , defined by

$$\Delta_R = \frac{|E_2 - E_1|}{|E_0|}. \quad \text{Eq. 7}$$

Figure 17 presents the relative differences between the simulator predictions and the FEKO predictions.

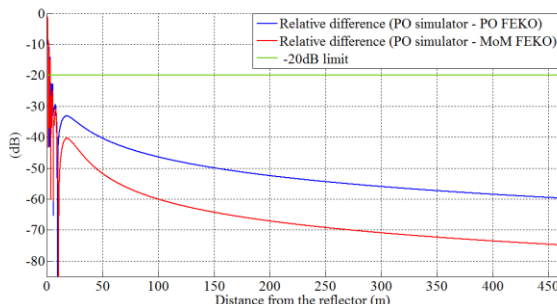


Figure 17 Relative difference of the first-order scattered field

We observe that except in the close vicinity of the façade, i.e. where Eq. 3 is not respected, the relative differences are below -20dB (Eq. 5). Hence the PO prediction is validated at two levels. Firstly, it fits with the PO prediction of FEKO, which validates the implantation of PO in the simulator. Secondly, it also fits with the MoM prediction of FEKO, which validates our method choice and shows that for first-order reflection predictions, PO can be considered as a reference method.

We now present the validation of the second-order reflection. We compare the field scattered by the two reflectors of scene 2. The computation has been done with the simulator and with the MoM method (FEKO). Notice that FEKO cannot compute reflections of multiple order with PO. Figure 18 and Figure 19 present the results.

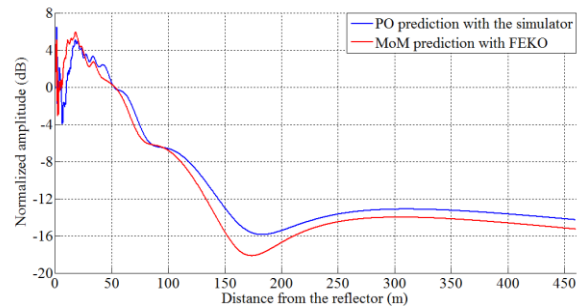


Figure 18 Comparison of the second-order scattered field computed with the simulator (blue), with FEKO using the MoM method (red)

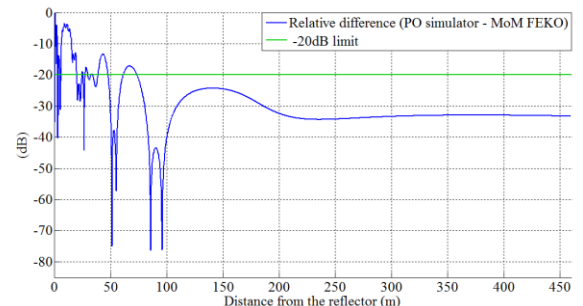


Figure 19 Relative difference of the second-order scattered field

We observe a good agreement between the two methods. The general behaviors are well reproduced and the levels are the same. However, as expected we observe larger differences than for the first-order reflection. Indeed, as explained previously, the second-order reflection is computed via a hybrid method using PO and GO. The use of GO in the propagation between the two reflectors may explain the slight differences.

The strongest difference is observed in the vicinity of the reflectors: it reaches -5dB for distances inferior to 15m. However, for greater distances, the difference becomes smaller, punctually for a distance of 43m it reaches -13dB, and then it is close or below -20dB. Finally, PO can be considered as a reference method also for second-order reflection predictions.

In this section the comparison PO/MoM via FEKO has been presented. This validates the PO simulator at two levels. Firstly, the comparison with the PO prediction of FEKO validates the implantation of PO in the simulator. Secondly, the comparison with MoM proves that we can consider PO as a reference method because the results are in good agreement.

V. COMPUTATION EFFICIENCY IMPROVEMENT

The aim of this section is to present our choices and techniques in order to improve the simulator efficiency.

Maximum order of reflections

One of the main issues when designing a multipath prediction simulator is to choose the maximal reflection order which has to be computed, because the determination of multiple reflections adds an important computation load. The simulator can compute reflections up to order 2. In this section we justify this choice.

For this purpose we compute the amplitude of the field reflected by a concrete reflector and by a glass reflector. Notice that the reflection is computed until the fourth order, i.e. after 4 reflections on concrete or glass reflectors.

The values of the ratio between the direct field amplitude and the four reflection orders are exposed in Table 1. As expected the reflected field amplitude decreases with respect to the reflection order.

Material Ratio (dB)	Concrete	Glass
Order 1 / Direct field	-7.2	-8
Order 2 / Direct field	-12.6	-15
Order 3 / Direct field	-17.5	-21
Order 4 / Direct field	-22.3	-27.1

Table 1 Amplitude ratio in dB between the direct field and the reflection orders up to 4

We observe that the ratio of the fourth order reflection is very weak since it is below to -20dB . Concerning the third order reflection we observe that the ratio is close to -20dB for concrete (-17.5dB) and glass (-21dB).

Note also that generally the reflection modifies the polarization. The direct field is purely right-hand circularly polarized (RHCP). Then, the first order reflection is mainly left-hand circularly polarized (LHCP), the second order is mainly RHCP, etc... Because the receiver antenna is RHCP, the field of reflections of order 1 and 3 are strongly attenuated by the antenna, while the direct field, the second and fourth order reflections are weakly attenuated. As to conclude, reflection of order 4 and superior are too weak to yield significant multipath ($< -20\text{dB}$). Reflections of order 3 are generally about -20dB below the direct field and they will be strongly attenuated by the antenna.

Considering the influence of the antenna, these results validate the computation of the reflection only up to order 2.

Minimum size of the objects in the scene

For objects smaller than 4λ (approx. 80cm), the PO prediction of the surface currents is potentially false as explained in [14]. Then, these objects should not be

modeled in the scene. This is a limit of the prediction simulator.

However, except in their close vicinity, the field scattered by such small objects is considerably weaker than the direct field or the field scattered by larger elements as buildings of the airport environment for instance. Indeed, as illustrated in Figure 20, we can see that the field reflected by a 0.8m object can be neglected in comparison to the field reflected by a 5m object. For distances above 35m the larger object yields reflected field at least 25dB greater.

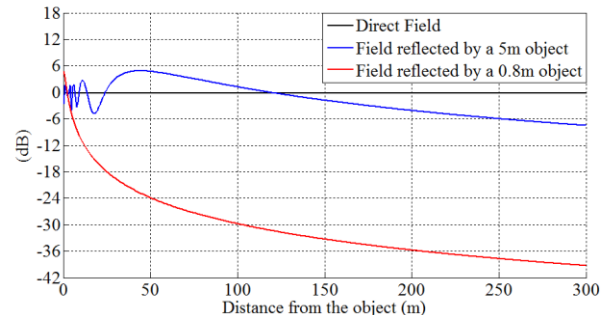


Figure 20 Reflected field in the specular direction for a 0.8m and 5m metallic object

Moreover, in dynamic situations, the influence of such small objects can clearly be neglected since the subsistence time of the multipath is very short.

Multipath reduction process

Since each illuminated facet generates a multipath, the computation load for the GPS receiver simulator can become important in case of a complex 3D scene. In order to reduce the number of multipath we group adjacent multipath.

In static situations, if (a_1, τ_1, ϕ_1) and (a_2, τ_2, ϕ_2) are the characteristics of two multipath to be grouped, they are reduced as one equivalent multipath defined by

$$a = |a_1 e^{j\phi_1} + a_2 e^{j\phi_2}|, \\ \tau = \frac{a_1^2 \tau_1 + a_2^2 \tau_2}{a_1^2 + a_2^2}, \\ \phi = \arg(a_1 e^{j\phi_1} + a_2 e^{j\phi_2}). \quad \text{Eq. 8}$$

We deduce that two multipath may be reduced to one multipath if the condition

$$ae^{j\phi} e^{-j2\pi f \tau} = a_1 e^{j\phi_1} e^{-j2\pi f \tau_1} + a_2 e^{j\phi_2} e^{-j2\pi f \tau_2}. \quad \text{Eq. 9}$$

is respected in the entire GPS band. Note that at the central frequency, i.e. $f = 0$, we find back the equivalent values for a and ϕ .

In order to get a simple mathematical expression we make the hypothesis $a_1 = a_2$ and Eq. 9 becomes

$$ae^{j\phi} e^{-j2\pi f\tau} = 2 a_1 \cos \left(\pi f(\tau_1 - \tau_2) + \frac{(\phi_1 - \phi_2)}{2} \right) e^{-j2\pi f \frac{(\tau_1 + \tau_2)}{2} - j\frac{(\phi_1 + \phi_2)}{2}}.$$

Eq. 10

The amplitude of the gathered multipath has to be constant on the whole GPS frequency band, i.e. the cosine factor has to be constant on the frequency band which leads to the necessary condition:

$$|B(\tau_1 - \tau_2)| \ll 1. \quad \text{Eq. 11}$$

where B is the bandwidth of the GPS L1 signal. Hence two multipath can be grouped only if their delays respect this condition.

In dynamic situations, the Doppler shifts of the direct signal and each multipath have to be taken into account. Hence, the Doppler shifts also have to be reduced. This adds a condition for the multipath reduction. Hence, if the Doppler shifts difference $\Delta f_d = f_{d1} - f_{d2}$ between two multipath is inferior to the Doppler-criterion D_c , they are reduced according to Eq. 12.

$$f_d = \frac{a_1^2 f_{d1} + a_2^2 f_{d2}}{a_1^2 + a_2^2}. \quad \text{Eq. 12}$$

The final reduction condition in dynamic cases is then

$$|B(\tau_1 - \tau_2)| \ll 1 \text{ and } \Delta f_d \leq D_c. \quad \text{Eq. 13}$$

Moreover, all the multipath with a delay such that

$$\tau > T_C + \frac{\delta_{E-L}}{2} \quad \text{Eq. 14}$$

are rejected since they do not have any influence on the GPS position [15]. In this expression, $T_C = 1/F_C$ where F_C is the GPS L1 C/A code frequency ($F_C = 1.023\text{Mhz}$) and δ_{E-L} is the early-minus-late chip spacing. For our application we consider a maximum chip spacing $\delta_{E-L} = T_C$, which leads to the conclusion that all the multipath with a delay such that

$$\tau > \frac{3}{2} T_C \quad \text{Eq. 15}$$

are rejected.

We now discuss the efficiency of the multipath reduction. For this purpose we have computed the number of multipath on a segment at 45m along a facade of size 10mx10m, for different facet sizes, with and without the multipath reduction process. Notice that according to Eq. 3, at this distance the maximum size of the facets is approximately 2m.

Figure 21 illustrates the number of computed multipath without the multipath reduction process (a) and with the

multipath reduction process (b), for 0.5m, 1m, 1.5m and 2m facets.

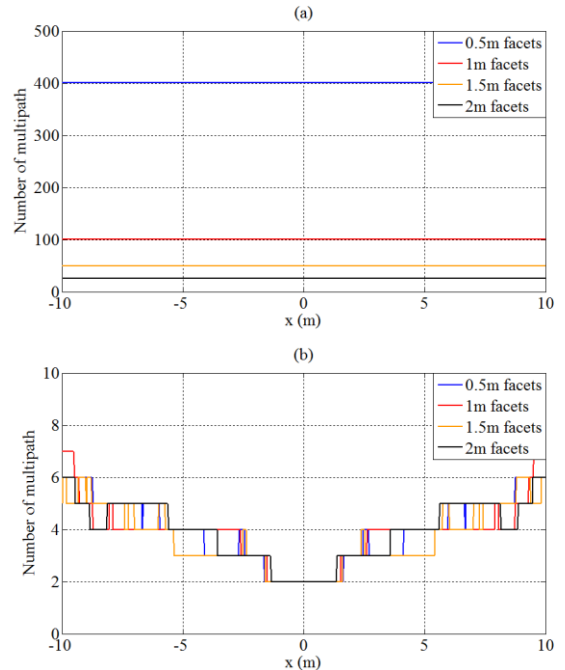


Figure 21 Number of multipath computed along a segment at 45m from a 10m x 10m façade, without (a) and with (b) the reduction process

First of all we observe that the reduction process leads to an important improvement since it drastically reduces the number of multipath. Indeed, for 0.5m facets their number is divided by a factor of minimum 60, and for the 1m, 1.5m, and 2m facets, it is divided by a factor of 10 approximately.

As expected, without the reduction process, for a given size of facets, the number of multipath is constant along the segment since the number of illuminated facets does not change, whereas it is variable when the reduction process is used.

As a conclusion, we notice that the multipath reduction process is really useful for predictions in complex scenes, in order to reduce the computation costs.

In order to validate the reduction process we compare the transfer functions of the multipath channel computed with and without the multipath reduction process for different size of facets. The scene configuration of the simulation is the same as the one used to compute the number of multipath, i.e. a 10mx10m metallic façade as illustrated in Figure 22. In order to respect Eq. 3, we observe at a minimum distance of 45m, since we compute the differences for facets of size 2m.

The satellite signal incidence is normal to the façade. We compute the root mean square difference in front of the façade (Eq. 4).

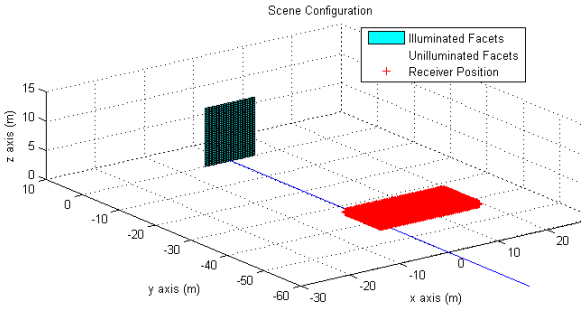


Figure 22 Scene configuration

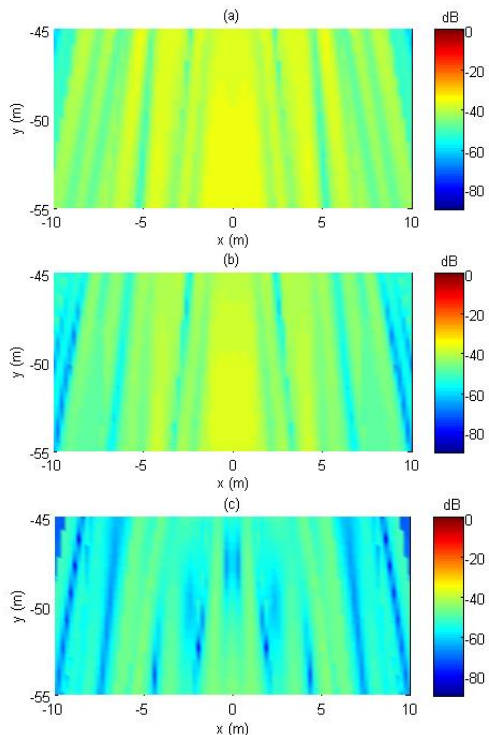


Figure 23 Root mean squared difference between the transfer functions obtained with and without the reduction process for (a) 0.5m, (b) 1m, (c) 2m facets

We observe that the differences are below -35dB everywhere regardless of the facet size. Hence we conclude that the multipath reduction process does not affect the validity of the multipath prediction.

GPS multipath area

Eq. 14 and Eq. 15 define a multipath delay limit above which a multipath does not affect the position estimation. Since T_C corresponds to a propagation distance of approximately 293 meters, multipath with a relative distance delay above 439.5 meters are not a source of positioning error. Hence we could define an area outside which the environment will not affect the position estimation. In the following we call this area the GPS multipath area. Such an area would be interesting since it limits the scene to take into account.

Nevertheless, Eq. 14 and Eq. 15 do not mean that an object further than 439.5 m from the receiver will not affect the positioning. In the following we note L_R the multipath relative delay. According to Figure 24 we have

$$L_R = (L_1 + L_2) - L_0. \quad \text{Eq. 16}$$

Figure 24 (a) illustrates the case where the multipath relative delay L_R is small while the antenna is far from the reflector. Whereas Figure 24 (b) illustrates the case where the multipath relative delay L_R is important while the antenna is close to the reflector.

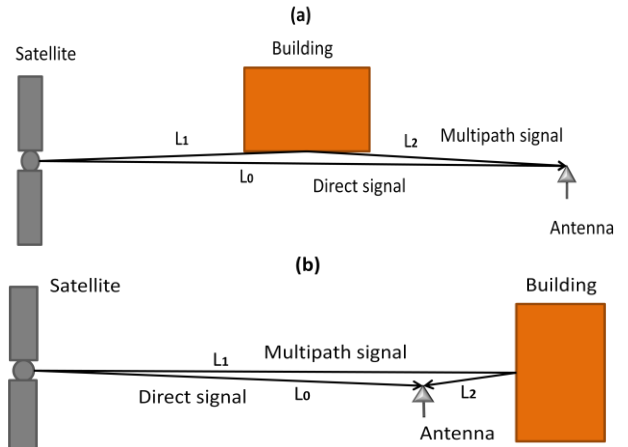


Figure 24 Relative delay of multipath in 2 configurations

Hence, it appears difficult to define rigorously a general multipath area valid for all simulations from the maximum multipath delay that affects the receiver. Then we simplify the problem starting from another geometrical aspect. Considering the mask angle α of the GPS satellites we can compute the maximum first order reflection illumination range in function of the height of a building.

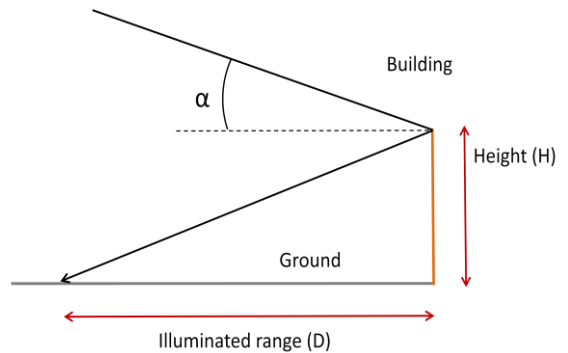


Figure 25 Illustration of the first-order illumination

With a maximum height $H_{max} = 40\text{m}$, and a mask angle $\alpha = 5^\circ$, we get

$$D_{max} \simeq 460\text{m}. \quad \text{Eq. 17}$$

Notice that such values for H and α can be considered as worst case values, especially for airport navigation applications. The obtained D_{max} is then a maximum

value. Therefore, we consider that 460m is the radius of the multipath area even if we do not take into account the second order reflection (e.g. ground reflection).

Harmonic hypothesis validation

As explained previously, the harmonic hypothesis is the fact that in the electromagnetic computation, everything is done as if the GPS signal was monofrequential of frequency $f = f_{L1}$, i.e. a pure sinusoidal signal. The question is to know how this hypothesis affects the multipath prediction in order to get validity conditions. In the following we expose the validation process.

We consider the scene illustrated by Figure 22. Firstly, we discretize the GPS frequency band (24Mhz centered on f_{L1}) and we compute the multipath channel for the scene with Eq. 1. Hence, we get the channel transfer function with the harmonic hypothesis. Secondly, we do the electromagnetic computation for each discretized frequency in order to obtain the transfer function without the harmonic hypothesis. In Figure 26, we compare the root mean square difference (Eq. 4) between the transfer functions with and without the harmonic hypothesis for 3 facet sizes.

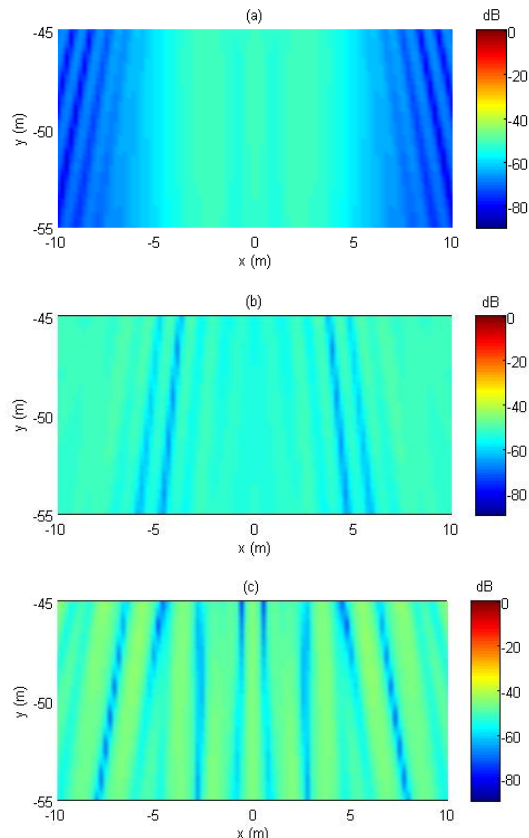


Figure 26 Comparison of the computed transfer functions with and without the harmonic hypothesis for (a) 0.5m, (b) 1m and (c) 2m facets

We observe that the differences are very small, below -39dB . Hence these results validate the harmonic hypothesis for facets of size smaller than 2m. We also notice that the smaller the facets are, the lower the error is. However, even for facets of 2m, the error remains acceptable.

Final choice of the settings for airport navigation

In this section we have presented different hypotheses and techniques to improve the computation efficiency. Here we summarize how the simulator can be used for airport applications.

Concerning, the facet size, a size of 1m seems to be a good trade-off. Firstly it reduces significantly the number of multipath in comparison with a 0.5m mesh as illustrated in Figure 21. Secondly, for facets of 1m, the minimal distance between any facet and the receiver is of 10m as illustrated in Figure 8. This is adapted to airport navigation since the GPS antenna of an airplane is never closer than 10m from the airport environment, even when the airplane is at a parking position.

Regarding the scene modeling, modeling the environment at distances shorter than 460m to the airplane trajectory is sufficient and objects smaller than 0.8m can be neglected.

VI. TEST-CASE SIMULATIONS

In this section we present a typical simulation performed with the simulator, and we illustrate the influence of the receiver dynamic on the range estimation error. As in [8] we perform simulations for an ENAC campus building.

Configuration

The building is made of concrete walls with glass windows. The ground is assumed to be asphalt and is modeled as planar and infinite of permittivity $\epsilon_r = 2.5 - j0.25$. We compute the multipath range error along a segment of length 110m at a distance of 30m from the façade. In the horizontal plane this segment has an angle of 3° with the façade. Its height is set to 8m in order to represent the average height of a GPS antenna onboard an airplane. The satellite elevation is of 8° . The scene is illustrated in Figure 27.

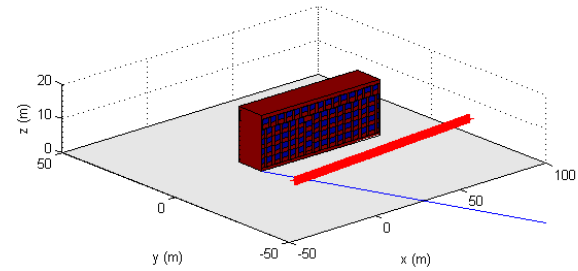


Figure 27 ENAC campus building

Concerning the GPS receiver simulator, the DLL bandwidth is set to 1Hz, the PLL bandwidth is set to 10Hz, the integration time is set to 20ms and the early minus late chip spacing is set to $0.4T_c$.

Results

In Figure 29, we display the range error obtained with an isotropic antenna in static and dynamic configurations. The dynamic configuration corresponds to a trajectory on the segment with a speed of 10m.s^{-1} .

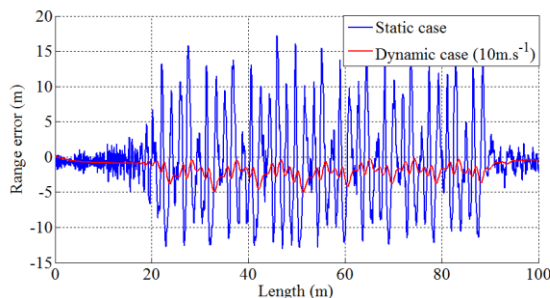


Figure 28 GPS C/A range error estimation with an isotropic antenna

In static configuration we observe that the range error presents numbers of oscillations between approximately $[-6\text{m}, 6\text{m}]$. On the other hand, in dynamic configuration we observe that the multipath error is smoothed. The remaining oscillations are due to the periodic structure of the building.

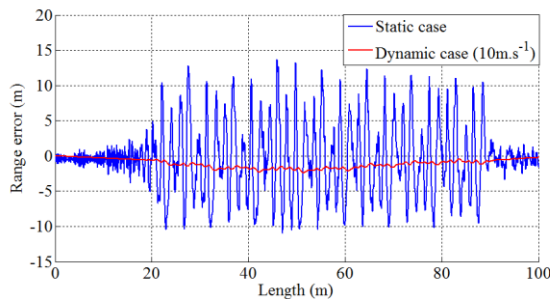


Figure 29 GPS C/A range error estimation with a realistic antenna

Next, we present the results obtained with a realistic GPS antenna. We observe that this antenna yields smaller range errors. This may be due to the fact that the multipath arriving from below the antenna, i.e. with a negative elevation, are strongly attenuated by the realistic antenna.

VII. CONCLUSION

In this article we have proposed a GPS multipath simulator adapted to airport navigation which can predict the GPS multipath error in static and dynamic configurations.

Concerning the electromagnetic modeling, it has been shown that in GPS context GO and UTD should not be used since the minimal acceptable size of objects that they can treat may be estimated at approximately 13m. Next, the choice of PO has been validated by means of comparisons with MoM.

Solutions have been proposed to improve the computation efficiency. For the scene modeling, we have shown that objects of size smaller than 80cm can be neglected. Regarding the multipath computation, we have verified the harmonic hypothesis which allows to do the electromagnetic computation as if the GPS signal were monofrequential of frequency $f = f_{L1}$. Also, we have exposed an efficient method to reduce the number of multipath and it has been shown that the computation of reflections order up to the second order are sufficient.

A test-case has been presented. We have observed differences between static and dynamic configurations. In dynamic situations the errors are smoothed and smaller. We have also observed the influence of the receiver antenna.

For future work, a complementary statistical prediction could be added to account for the lack of knowledge of the environment.

ACKNOWLEDGMENTS

The authors wish to thank Airbus for funding this work.

REFERENCES

- [1] R.Ercek, P. De Doncker, F. Grenez, "Study of pseudo-range error due to non-line-of-sight-multipath in urban canyons," in *Proc. ION GNSS*, Sept. 2005.
- [2] J. Legenne, J-J. De Ridder, "Performance of satellite navigation in urban areas with augmentations and hybridizations," in *Proc. ENC GNSS*, Apr. 2003.
- [3] H. Suzuki, "A statistical model for urban radio propagation," *IEEE Transactions on Communications*, vol. Com-25, no.7, Jul. 1977.
- [4] G.L. Turin, F.D. Clapp, T.L. Johnston, S.B. Fine, "A statistical model of urban multipath propagation," *IEEE Trans. on Vehicular Technology*, vol. VT-21, no. 1, Feb. 1972.
- [5] R.Ercek, P. De Doncker, F. Grenez, "Statistical determination of the pseudo-range error due to non-line-of-sight-multipath in urban canyons," in *Proc. ION GNSS*, Sept. 2006.
- [6] A. Steingaß, A. Lehner, F. Pérez-Fontán, E. Kubista, M.J. Martín, B. Arbesser-Rastburg, "The high resolution aeronautical multipath navigation channel", *IEEE PLANS*, Apr. 2004.

- [7] O. Esbri-Rodriguez, A. Konovaltsev, A. Hornbostel, "Modeling of the GNSS directional radio channel in urban areas based on synthetic environments," in *Proc. ION NTM*, Jan. 2004.
- [8] A. Chen, A. Chabory, A.C. Escher, C. Macabiau, "Comparisons of Multipath Modeling Strategies for the Estimation of GPS Positioning Error," in *Proc. EUCAP*, Berlin (Germany), March 2009
- [9] E. D. Kaplan et al, "*Understanding GPS: principles and applications*," Artech House, 1996.
- [10] <http://www.feko.info/feko-product-info>
- [11] S.W. Lee, R.M. Mittra, "Fourier transform of a polygonal shape and its application in electromagnetics," *IEEE Trans. on Antennas and Propagation*, vol. AP-31, no.1, Jan. 1983.
- [12] C. Macabiau, B. Roturier, E. Chatre, A. Renard, "Airport multipath simulation for sitting DGPS reference stations," in *Proc. ION NTM*, Jan. 1999.
- [13] D. A. McNamara, C.W. I. Pistorius, J. A. G. Malherbe, "*Introduction to The Uniform Geometrical Theory Of Diffraction*", Norwood, MA: Artech House, 1990.
- [14] S. Laybros, "Utilisation du lancer de rayons pour le calcul de l'interaction d'un rayonnement électromagnétique avec des objets complexes métalliques et diélectriques", PhD. Thesis, Université de Toulouse Paul Sabatier, Oct. 2004.
- [15] C. Macabiau, B. Roturier, A. Benhallam, E. Chartre, "Performance of GPS receivers with more than one multipath," in *Proc. ION NTM*, Sept. 1999.